CHEMISTRY
A EUROPEAN JOURNAL

DOI: 10.1002/chem.200801041

Tetraethylenepentamine-Directed Controllable Synthesis of Wurtzite ZnSe Nanostructures with Tunable Morphology

Baojuan Xi, Shenglin Xiong,* Dechen Xu, Jingfa Li, Hongyang Zhou, Jun Pan, Jiangying Li, and Yitai Qian*[a]

Abstract: A novel tetraethylenepentamine (TEPA)-directed method has been successfully developed for the controlled synthesis of ZnSe particles with distinctive morphologies, including nanobelts, nanowires, and hierarchically solid/hollow spheres. These structures, self-assembled from nanobelts and nanorods, have been synthesized by adjusting the reaction parameters, such as the solvent composition, reaction temperature, and the aging time. Results reveal that the volume ratio of H_2O and TEPA plays a crucial role in the final morphology of ZnSe products. The mechanisms of phase formation and morphology control of ZnSe particles are proposed and discussed in detail. The products have been characterized by means of X-ray diffraction, field-emission scanning electron microscopy, transmission electron microscopy (TEM), selected area electron diffraction, high-resolution TEM, Raman spectra and luminescence spectroscopy. The as-prepared ZnSe nanoparticles display shape- and size-dependent photoluminescent optical properties. This is the first time to report preparation of complex hollow structures of ZnSe crystals with hierarchy through a simple solution-based route. This synthetic route is designed to exploit a new H_2O/TEPA/N_2H_4·H_2O system possibly for the preparation of other semiconductor nanomaterials.

Keywords: hierarchical · nanobelts · nanowires · photoluminescence · spheres · tetraethylenepentamine

Introduction

As we know, manipulating the shape of nanocrystals provides a way to tune their properties. Among a variety of strategies for controlled synthesis, the solution-based chemical process is an effective method to fabricate nanostructural materials with well-defined shapes, sizes, and structures.[1] For instance, various chalcogenide-semiconductor nanomaterials with desired shapes and crystal phases were gained through the solution-based route.[2] As an important II–VI semiconductor, with a room-temperature bulk band-gap of 2.70 eV (460 nm), ZnSe-based nanostructures have been the subject of intense interest in view of their wide-ranging applications as light-emitting diodes (LEDs), lasers emitting in the blue range, and photodetectors[3] owing to significantly large exciton binding energy (21 meV[4]) in comparison to GaAs (4.2 meV[5]).

Diverse ZnSe nanostructures, including nanowires,[6] nanobelts,[7] nanotubes,[8] tertrapod nanorods,[9] and microspheres,[10] have thus attracted intense attention originating from their potential applications as optoelectronic materials. Recently, selectively preparing 1D to 3D semiconductor nanostructures represents some exciting progress.[11] However, no work on a one-pot preparation of ZnSe from 1D to 3D nanostructures in solution has been reported to date. Accordingly, to develop facile chemical methods suitable for selectively synthesizing ZnSe 1D and 3D complex nanoarchitectures still remains a great challenge.

The amine could more strongly bond to a particular surface facet of some semiconductor nanocrystals, such as ZnSe, and promote their precipitation on the more weakly passivated surfaces, which can make some nanostructures with novel morphology form. Therefore, monoamine- or polyamine-based template technique[11b–c,12] has broad application in the synthesis of various nanostructures. Inspired by

[a] Dr. B. Xi, Dr. S. Xiong, Dr. D. Xu, J. Li, Dr. H. Zhou, Dr. J. Pan, Dr. J. Li, Prof. Y. Qian
Department of Chemistry
Hefei National Laboratory for Physical Sciences at Microscale and Department of Materials Science & Engineering
University of Science and Technology of China
Hefei, Anhui, 230026 (China)
Fax: (+86) 551-3607402
E-mail: xsl8291@ustc.edu.cn
ytqian@ustc.edu.cn

Supporting information for this article is available on the WWW under http://dx.doi.org/10.1002/chem.200801041.

WILEY InterScience DISCOVER SOMETHING GREAT
© 2008 Wiley-VCH Verlag GmbH & Co. KGaA, Weinheim

the technique, we designed a new tetraethylenepentamine (TEPA)-assisted method to prepare ZnSe nanostructures. Based on the TEPA-templated technique, we have successfully gained ZnSe materials from 1D to 3D nanostructures, including nanobelts, nanowires, and hierarchical spheres by nanobelt (or nanorod) self-assembly, by manipulating the reaction conditions. To the best of our knowledge, this is the first time for the one-step solution-based synthesis of novel ZnSe hierarchically hollow/solid microspheres by nanorod/nanobelt self-assembly. In addition, the optical properties of ZnSe nanoparticles with different shapes and sizes have been investigated here.

Results and Discussion

Structural determination and characterization of nanobelts and nanowires: Zinc selenide (ZnSe) nanobelts were prepared by TEPA-assisted solvothermal method with a volume ratio of $V_{H_2O}/V_{TEPA}/V_{N_2H_4\cdot H_2O}=20:30:5$ at 180 °C for 20 h. The X-ray diffraction (XRD) pattern of the obtained ZnSe product is shown in Figure 1b. All the reflection peaks can be indexed as wurtzite ZnSe with lattice constants $a=$ 3.97 Å and $c=6.52$ Å, which is in agreement with the literature values (JCPDS Card No. 80–008). No peaks of impurities were detected, revealing the high purity of the as-synthesized products.

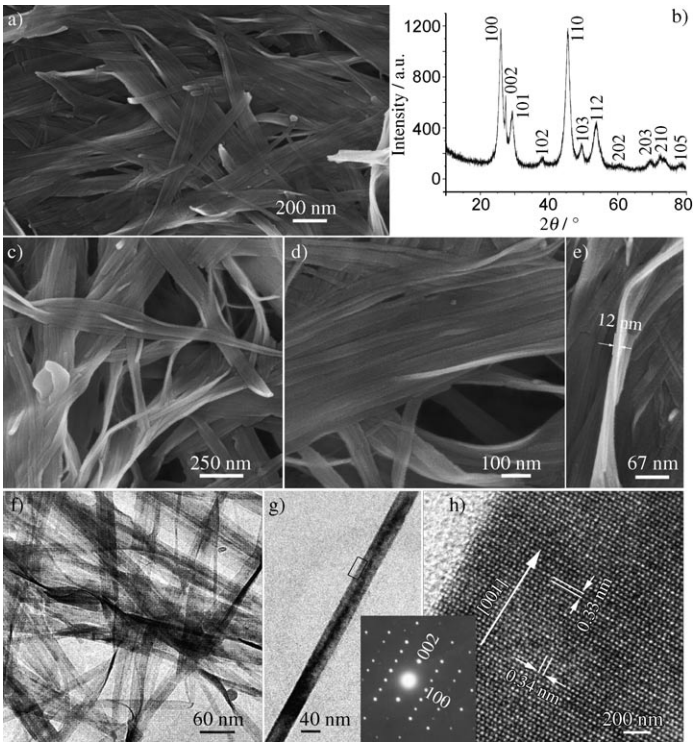

Figure 1. a) A low-magnification FESEM image of the ZnSe nanobelts, indicating lengths of up to several micrometers. b) A typical XRD pattern of the as-prepared ZnSe nanobelts. c–e) High-magnification FESEM images of the ZnSe product. f) A typical TEM image of the ZnSe nanobelts. g) TEM image of a single ZnSe nanobelt. h) HRTEM image of the selected area in (g). The inset of (g,h) shows its corresponding SAED pattern.

To make clear the morphology of ZnSe product, the sample was characterized by field-emission scanning electron microscopy (FESEM). The overview image in Figure 1a demonstrates the large-scale synthesis of nanobelts with length up to several micrometers. The more structure information is supported by the high-magnification images in Figure 1c–e, revealing the typical thickness in the range of 10–18 nm and width of 30 to 100 nm. A SEM image (Figure 1e) depicts a ribbon with thickness of about 13 nm and a characteristic rectangular cross-section. The high-magnification TEM image (Supporting Information, Figure S1) also shows that a flexible nanobelt with thickness of about 14 nm, which is agreement with the observation of SEM. Energy dispersive X-ray spectroscopy (EDS) analysis, represented in Figure S2 in the Supporting Information, reveals the presence of Zn and Se with an atomic ratio close to 1:1 (the O signal derives from the surface absorption of nanobelts and the Cu signal comes from the copper grid). By examining the nanobelts in detail, we found that these belts show a bundlelike shape (Figure 1a,d).

The results of XPS and Raman spectra identify the sample of nanobelts as hexagonal ZnSe of high crystallinity and purity (Supporting Information, Figure S3 and S4). To shed light on the more detailed structure of ZnSe nanobelts, HRTEM and selected-area electron diffraction (SAED) are further performed to examine the product. A typical low-magnification TEM image of ZnSe nanobelts is presented in Figure 1f. The selected-area electron diffraction (SAED) pattern (inserted in Figure 1f–g), taken from the single nanobelt in Figure 1g, exhibits a set of sharp spots and confirms that the nanobelts are single crystalline and can be indexed as the hexagonal ZnSe phase. Shown in Figure 1h is a HRTEM image recorded near the edge of this ZnSe nanoribbon. The regular spacings of the observed lattice planes are $\approx$0.33 and 0.34 nm, consistent with the separation of (002) and (100) planes of hexagonal ZnSe, respectively. The results demonstrate that the nanobelts grow preferentially along the [001] direction.

As for the synthesis of ZnSe nanostructures, reaction temperature plays an important role in determining the morphology of products. If the temperature was higher than 180 °C, then ZnSe nanowires rather than nanobelts were obtained. The TEM and HRTEM images of the sample obtained at 200 °C are shown in Figure 2. The panoramic morphology of the prepared nanowires is shown in Figure 2a in which we can observe bunched, flexible, ultrathin nanowires with a uniform diameter. Shown in Figure 2b is a TEM image of an individual ZnSe nanowire with a diameter of 18 nm. The fast Fourier-transformation electron diffraction (FFT ED) pattern (inserted in Figure 2b) and the corresponding high-resolution TEM image of the nanowire (Figure 2c) confirms the single-crystal nature and the preferential growth along [001] direction, similar to that of ZnSe nanobelts, revealing the same growth process of nanobelts and nanowires.

 © 2008 Wiley-VCH Verlag GmbH & Co. KGaA, Weinheim

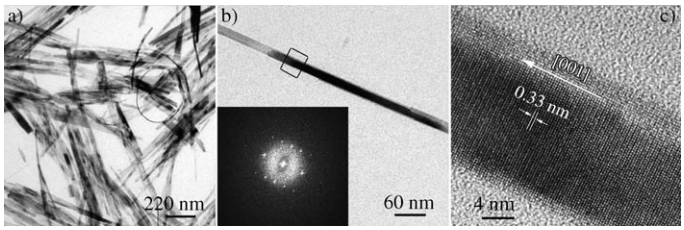

Figure 2. ZnSe nanowires fabricated through a TEPA-assisted solvothermal method with a volume ratio of $V_{H_2O}/V_{TEPA}/V_{N_2H_4\cdot H_2O}=35:15:5$ at 220 °C for 20 h: a) Low-magnification SEM image of the nanowires, b) TEM image of a single ZnSe nanowire. c) HRTEM image of the selected area in (b). The inset indicates its corresponding FFT ED.

Characterization of ZnSe microspheres: Control experiment analysis reveals that the manipulation of ZnSe morphology is intensively dependent on the composition of mixed solution, such as the volume ratio of H_2O and TEPA and reaction temperature. The conditions for preparing some typical samples by varying the component ratios of the mixed solution are listed in Table 1 (also see the Supporting Information, Figure S5–S8). The H_2O-TEPA ratio determines the products final morphology and structure, but without changing the products crystal phase, which could be demonstrated by XRD patterns of the products prepared under different volume ratios of H_2O and TEPA (Supporting Information, Figure S9). An appropriate volume ratio of H_2O/TEPA is crucial to the construction of given nanostructures. When the volume ratio of H_2O dominates, i.e., $V_{H_2O}:V_{TEPA}=9:1$, what has been obtained is shown in Figure 3, presenting that the products consist of nearly monodisperse microspheres by self-assembly of ultrathin, flexible nanobelt arrays (see Figure 3a–b). If the reaction temperature increased to 240 °C, the obtained sample was found to contain ZnSe microspheres constructed with nanorod arrays as shown in the Figure 3c–d.

Table 1. Summary of experimental results indicating the influence of the composition of a mixed solution and reaction temperature on shape of the products.

$V_{H_2O}/V_{TEPA}/V_{N_2H_4\cdot H_2O}$	T [°C]	t [h]	Morphology
20:30:5	180	20	nanobelt arrays
30:20:5	180	20	nanobelts
35:15:5	180	20	nanobelts
35:15:5	200	20	nanowires
40:10:1	180	20	spheres by nanobelt bundle self-assembly
45:5:1	160	20	hierarchical spheres by nanobelts self-assembly
45:5:1	200	20	spheres by nanobelt array self-assembly
45:5:1	200	36	spheres by nanorod array self-assembly
45:5:1	240	20	spheres by nanorod array self-assembly
45:5:1	240	36	hollow spheres by nanorod array self-assembly

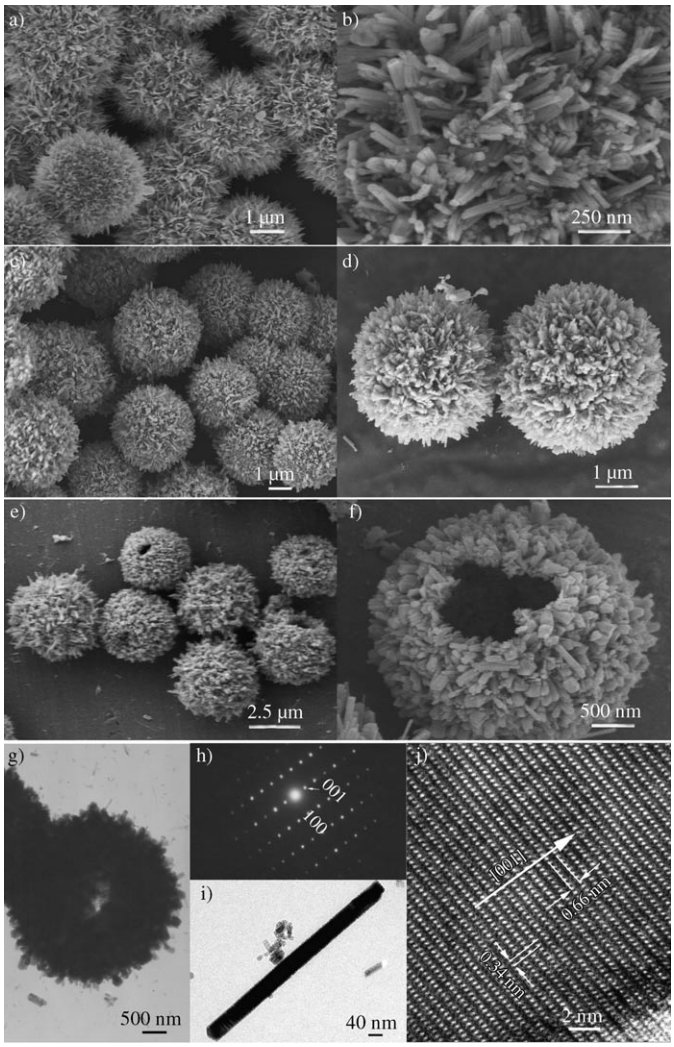

Figure 3. a–f) FESEM images of ZnSe microspheres constructed from the self-assembly of nanobelt arrays prepared in a mixed solution with $V_{H_2O}/V_{TEPA}/V_{N_2H_4\cdot H_2O}=45:5:1$. a–b) at 200 °C for 20 h. c–d) 240 °C for 20 h. e–f) 240 °C for 36 h. g) TEM image of a typical hierarchical hollow sphere. h–i) the TEM image and SAED pattern obtained from a single nanorod of hollow sphere. j) HRTEM image recorded near the edge of the particular nanorod.

With respect to the synthesis of ZnSe nanostructures, the reaction time also exercises a significant influence on the morphology of products. Surprisingly, if only the reaction time was prolonged to 36 h with other conditions kept unchanged, ZnSe hollow microspheres instead of solid microspheres were produced. The FESEM images of the sample obtained at 240 °C for 36 h, indicating ZnSe product takes on hierarchically hollow urchin-like morphology can be seen in Figure 3e,f. Close observations of a typical broken urchin-like structure (Figure 3f) reveals that the sphere was constructed from tightly self-assembled nanorod arrays aligned perpendicularly to the surface of the urchin spheres with diameter of about 3–4 μm. The hollow nature of these spheres can also be confirmed by a TEM image (Figure 3g). Studies of he HRTEM image and SAED pattern (Figure 3h–j) dem-

 © 2008 Wiley-VCH Verlag GmbH & Co. KGaA, Weinheim

onstrate that the individual nanorod is single crystal and grows along [001] direction.

Growth process and formation mechanism of ZnSe nanobelts: As discussed above, the solution composition, i.e., the volume ratio of H_2O and TEPA, reaction temperature, and aging time all affect the morphology of products. The formation of nanobelt arrays (or mirospheres) is possible only within a very narrow composition range of the mixed solution, suggesting that the presence of TEPA plays a crucial role in the formation of such elegant and novel ZnSe nanostructures.

To investigate the growth process of these nanobelts, a series of experiments were carried out, as discussed below. We followed the nucleation and growth steps by studying the samples obtained at different reaction stages using the TEM and XRD techniques. Figure 4a–d shows the TEM images of the samples obtained after the reaction performed for 30 min, 1 h, 3 h, and 9 h, respectively. These images distinctly reveal the transformation process of the particle morphology from the mixture of particles and urchinlike spheres to nearly monodisperse urchinlike spheres, to nanobelts network, and finally to nanobelts.

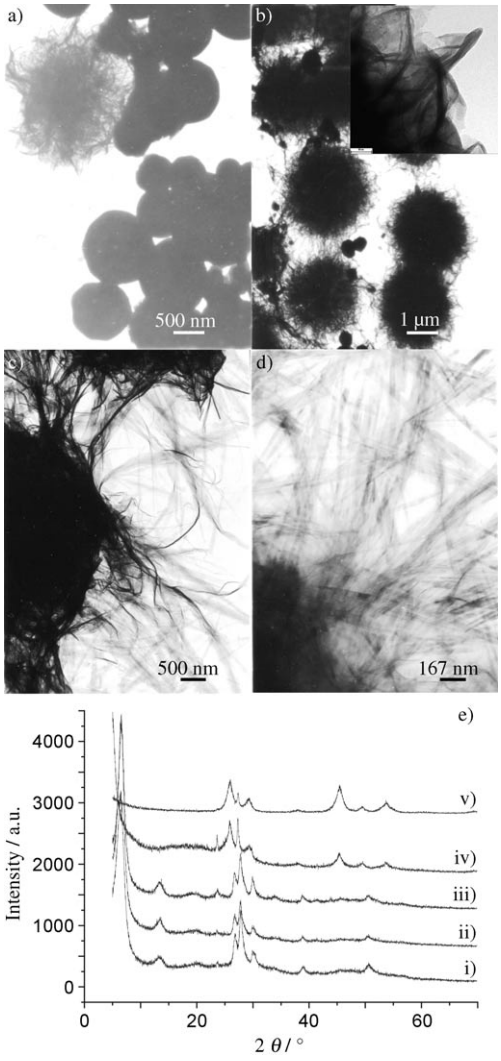

Figure 4. TEM images of the ZnSe nanobelts obtained at 180 °C for a) 30 min, b) 60 min, c) 2 h, and d) 6 h. e) XRD pattern of ZnSe nanobelts prepared at 180 °C for i) 30 min, ii) 60 min, iii) 2 h, iv) 6 h, and v) 10 h.

Figure 4a shows the TEM image of the product obtained after 30 min, which reveals the product consisted of the mixture of particles and urchinlike spheres. If the reaction time was prolonged to 60 min, nearly monodisperse urchinlike spheres predominated (Figure 4b) and the particles that appeared in Figure 4a vanished almost completely. High-magnification TEM image (see the panel inserted in Figure 4b) clearly reveals that urchinlike sphere is composed of lamellas, which tend to grow preferentially into nanobelts. If the reaction time was increased to 2 h, the morphology of the product changed remarkably. As shown in Figure 4c, the product consists of nanobelt networks constructed of ultrathin, flexible nanobelts. The nanobelts continue to grow preferentially and protrude toward the outside of netlike sphere-cores through the Ostwald-ripening process. Following this ripening process, these nanobelts gradually increased in quantity and finally nanobelt arrays predominate in the same region on the surface of the TEM grid (Figure 4d).

Time-dependent XRD patterns (see Figure 4e) reveal that phase transformation from precursor to ZnSe takes at least 6 h to complete, which means no ZnSe is formed initially. Taking into consideration the medium coordination ability of amine with metallic ions, the sample obtained at 180 °C for 30–120 min may be TEPA-intercalated ZnSe. FTIR analysis also demonstrates that the TEPA molecules may intercalate into the complex (Supporting Information, Figure S10). On the basis of the experimental results, the chemical formula of the precursor is assumed to be [ZnSe]-$(TEPA)_x$. Calculations based on the TGA results gave a value of $x = 0.5$ for the precursor within experimental error (Supporting Information, Figure S11). That is, [ZnSe]-$(TEPA)_{0.5}$ could serve as the precursor to ZnSe, similar to those of previous structures.[13] If the reaction time was prolonged to 6 h, the wurtzite ZnSe could be detected in the XRD pattern (Figure 4e–v). The characteristic peaks of ZnSe were remarkably intensified and those of the precursor were weakened and finally disappeared when the reaction time extended to 10 h (Figure 4e). These phenomena could be interpreted by the fact that longer growth time could result in the formation of nanocrystals that are thermodynamically stable. To make a summary, the formation procedure of the ZnSe nanobelts can seen in Equations (1) and (2):

$$Zn^{2+} + SeO_2 + TEPA \xrightarrow{N_2H_4 \cdot H_2O} [ZnSe](TEPA)_{0.5} + N_2 \quad (1)$$

$$[ZnSe](TEPA)_{0.5} \rightarrow ZnSe \quad (2)$$

On the basis of the above results and analyses, a possible ligand (TEPA)-assisted solid–solid growth mechanism (LSS)

 © 2008 Wiley-VCH Verlag GmbH & Co. KGaA, Weinheim

was proposed to explain the formation of the ultrathin, flexible ZnSe nanobelts. The formation of precursor [ZnSe]-$(TEPA)_{0.5}$ can be regarded as a crucial step for the formation of ZnSe nanobelts. The whole process is a special in situ decomposition of the precursor–urchinlike spheres composed of lamellas through a solid–solid phase transition in Equation (1), providing ZnSe units, which served as the seeds for the following growth of ZnSe nanobelts.

A High-magnification TEM image inserted in Figure 4b clearly reveals several short nanobelts that have grown from the lamellas. In this solid–solid transformation, the morphology of the final products was determined by the characteristic of the inherent chain type structure of TEPA, which could serve as a structure-directing coordination template. In fact, in most reported colloidal synthesis of metal or semiconductor 1D nanocrystals, the anisotropic growth of the 1D structure is often driven by using capping ligands that can bind selectively onto particular facets of the seed particles.[14] On the other hand, the specific crystal structure of wurtzite ZnSe may be another advantageous factor in the formation of one-dimensional beltlike nanostructure.

Formation of ZnSe microspheres: In the preparation of ZnSe nanobelts discussed above, the as-prepared products consist of only large aggregates composed of particles, without the use of TEPA. This result implies that the existence of TEPA favors the formation of ZnSe nanorods and further self-assembly in an ordered and tight manner, to form regular spheres in which TEPA molecules probably form interparticle bilayers inducing the ZnSe nanorods to glue together parallel during the self-assembly process. Recently, a similar self-assembly process of joining disordered inorganic nanoparticles to form ordered superstructures helped by organic molecules as linkers has been reported.[15] As a result, concerning the formation of ZnSe spheres self-assembled by nanobelts/nanorods in this study, effective self-assembly is induced by the linear molecular structure of TEPA through the special ZnSe atomic-surface structure, structure matching and spatial proximity. This self-assembly process is likely driven by energy minimization for the surfaces of nanobelts/nanorods.

With respect to the formation of hollow structures for ZnSe hierarchical spheres, the bubbles of N_2 gas generated by reduction of $N_2H_4{\cdot}H_2O$ in the reaction system must have played a significant role. In fact, the gas bubble-template method has been demonstrated to be effective for the preparation of hollow spheres.[10a,16] Hence, in this case, an energy-minimizing driven self-assembly of ZnSe nanorods on the base of N_2 bubbles induced by TEPA is responsible for the formation of hierarchically hollow spheres. According to Equation (1), many gas bubbles of N_2 produced in the reaction provide the aggregation center, that is, a soft-template. Simultaneously driven by the minimization of interfacial energy, small ZnSe nanocrystals may aggregate around the gas-liquid interface between N_2 and liquid, and then the nanocrystals grow on the surface of spheres gradually, which may result from the templating effect of TEPA and the specific crystal structure of wurtzite ZnSe. ZnSe hollow spheres may form through nanorod self-assembly.

Optical properties: The room-temperature photoluminescence spectra ($\lambda_{exc.}=365$ nm) of as-prepared ZnSe nanobelts and hierarchically hollow spheres were reordered to investigate their optical properties (Figure 5). Figure 5a show three

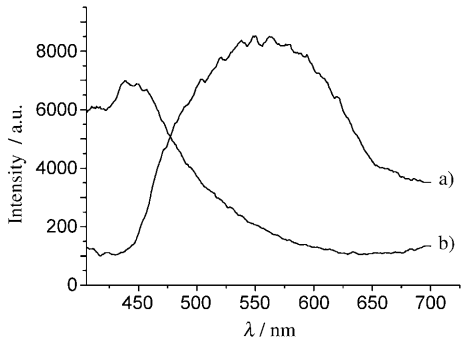

Figure 5. Photoluminescence spectra of as-prepared products. a) ZnSe nanobelts; b) ZnSe hierarchically hollow spheres by nanorod self-assembly.

strong emission bands at around $\lambda=438$, 449, and 457 nm, respectively. These emission bands are usually attributed to the edge emission of ZnSe.[17] Although, the photoluminescence spectrum of the ZnSe hierarchically hollow spheres displays a broad and strong emission peak in low energy level of $\lambda=500$–700 nm, the lower-energy emission of about $\lambda=550$ nm usually resulted from Zn-vacancy or impurities.[16–18]

Conclusions

Semiconductor wurtzite ZnSe nanocrystals with well-controlled shapes, including nanobelts, nanowires, solid or hollow microspheres assembled from nanobelts or nanorods, have been successfully prepared by a novel tetraethylenepentamine (TEPA)-directed solvothermal method. The effect of reaction conditions including the volume ratio of the mixed solvents, reaction temperature, and the aging time on the morphology of ZnSe was investigated in detail. Experimental results demonstrate that the volume ratio of H_2O and TEPA played a key role in determining the shape and size of the ZnSe products. On the basis of a series of transmission electron microscopy and XRD characterization analyses, a possible ligand (TEPA)-assisted solid–solid growth mechanism (LSS) was proposed to explain the formation of the ultrathin, flexible ZnSe nanobelts. An energy-minimizing-driven self-assembly of ZnSe nanorods with N_2 bubbles induced by TEPA, as soft template, is responsible for the formation of ZnSe hierarchically hollow spheres. To the best of our knowledge, this is the first time this kind of ZnSe hollow/solid superstructure has been synthesized in this way. The present work gives inspiration to the controlla-

 © 2008 Wiley-VCH Verlag GmbH & Co. KGaA, Weinheim

ble synthesis of other semiconductor nano- and micromaterials.

Experimental Section

Materials and preparation: The $Zn(Ac)_2{\cdot}2H_2O$ (99.0%, Aldrich), SeO_2 (99.0%, Aldrich), $N_2H_4{\cdot}H_2O$, and tetraethylenepentamine (TEPA) used were of analytical grade. All chemicals were analytical grade, commercially available from Shanghai Chemical Reagent, and used in this study without further purification. In a typical procedure, $Zn(Ac)_2{\cdot}2H_2O$ (1 mmol) and SeO_2 (1 mmol) were added to a given amount of distilled water and the mixture was dispersed to form a homogeneous solution by constant strong stirring. Then, a given amount of TEPA and hydrazine hydrate ($N_2H_4{\cdot}H_2O$) was added to the above solution at room temperature and continually stirred for 10 min. The resulting mixture was transferred into a Teflon-lined stainless autoclave (60 mL capacity). The autoclave was sealed and maintained at $T = 180$–$240\,^{\circ}C$ for 24 h. The system was then allowed to cool ambient temperature. The final product was collected and washed with distilled water and absolute alcohol several times, vacuum-dried, and kept for further characterization.

Characterization: The products were characterized by X-ray diffraction (XRD) recorded by using a Japanese Rigaku D/max-γA rotating anode X-ray diffractometer equipped with the monochromatic high-intensity $Cu_{K\alpha}$ radiation ($\lambda = 1.54178$). SEM images were taken with a field emission scanning electron microscope (FESEM, JEOL-6300F, 15 kV). Microscopy was performed by using a Hitachi (Tokyo, Japan) H-800 transmission electron microscope (TEM) at an accelerating voltage of 200 kV, and a JEOL-2010 high-resolution TEM, also at 200 kV. X-ray photoelectron spectroscopy (XPS) measurements were performed by means of a VGESCALAB MKII X-ray photoelectron spectrometer with an $Mg_{K\alpha}$ excitation source (1253.6 eV). Raman spectra were recorded by using a Jobin Yvon (France) LABRAM-HR confocal laser micro-Raman spectrometer at room temperature. Photoluminescence (PL) measurements were carried out by using a Perkin–Elmer LS-55 luminescence spectrometer with a pulsed Xe lamp.

Acknowledgements

The financial support of this work, by the China Postdoctoral Science Foundation (20070420124), the K. C. Wong Education Foundation of Chinese Academy of Sciences, National Natural Science Foundation of China (No. 20431020) and the 973 Project of China (No. 2005CB623601), is gratefully acknowledged.

[1] a) B. L. Cushing, V. L. Kolesnichenko; C. J. O'Connor, *Chem. Rev.* **2004**, *104*, 3893; C. J. O'Connor, *Chem. Rev.* **2004**, *104*, 3893; b) X. Wang, J. Zhuang, Q. Peng, Y. Li, *Nature* **2005**, *437*, 121; c) H. Song, R. M. Rioux, J. D. Hoefelmeyer, R. Komor, K. Niesz, M. Grass, P. D. Yang, G. A. Somorjia, *J. Am. Chem. Soc.* **2006**, *128*, 3027.

[2] a) Z. A. Peng, X. Peng, *J. Am. Chem. Soc.* **2002**, *124*, 3343; b) N. Duxin, F. Liu, H. Vali, A. Eisenberg, *J. Am. Chem. Soc.* **2005**, *127*, 10063; c) L. Zhang, J. C. Yu, M. Mo, L. Wu, Q. Li, K. W. Kwong, *J. Am. Chem. Soc.* **2004**, *126*, 8116; d) I. Gur, N. A. Fromer, M. L. Geier, Alivisatos, A. P. *Science* **2005**, *310*, 462.

[3] a) M. A. Haase, J. Qiu, J. M. Depuydt, and H. Cheng, *Appl. Phys. Lett.* **1991**, *59*, 1272; b) R. Passler, E. Griebl, H. Ripel, G. Lautner etal. , *J. Appl. Phys.* **1999**, *86*, 4403; c) J. Wang, D. C. Hutchings, A. Miller et al., *J. Appl. Phys.* **1993**, *73*, 4746.

[4] Z. M. Zhu, N. Z. Liu, G. H. Li, H. X. Han, Z. P. Wang, S. Z. Wang, L. He, R. B. Ji, Y. Wu, *Int. J. Infrared Millimeter Waves* **1999**, *18*, 13.

[5] S. Z. Wang, S. F. Yoon, L. He, X. C. Shen, *J. Appl. Phys.* **2001**, *90*, 2314.

[6] a) X. F. Duan, C. M. Lieber, *Adv. Mater.* **2000**, *12*, 298; b) R. Solanki, J. Huo, J. L. Freeouf, *Appl. Phys. Lett.* **2002**, *81*, 3864; c) Y. C. Zhu, Y. Bando, *Chem. Phys. Lett.* **2003**, *377*, 367; d) Q. Li, X. G. Gong, C. R. Wang, J. Wang, K. Ip, S. Hark. *Adv. Mater.* **2004**, *16*, 1436; e) S. L. Xiong, J. M. Shen, Q. Xie, Y. Q. Gao, Q. Tang, Y. T. Qian, *Adv. Funct. Mater.* **2005**, *15*, 1787; f) Y. Cai, S. K. Chan, I. K. Sou, Y. F. Chan, D. S. Su. N. Wang, *Small* **2007**, *3*, 111; g) A. G. Dong, R. Tang, W. E. Buhro, *J. Am. Chem. Soc.* **2007**, *129*, 12254; h) D. D. Fanfair, B. A. Korgel, *Chem. Mater. 2007, 19*, 4943.

[7] a) Y. Jiang, X. M. Meng, W. C. Yiu, J. Liu, J. X. Ding, C. S. Lee, S. T. Lee, *J. Phys. Chem.* B **2004**, *108*, 2787; b) S. L. Xiong, B. J. Xi, C. M. Wang, G. C. Xi, X. Y. Liu, Y. T. Qain, *Chem. Eur. J.* **2007**, *13*, 7926; c) Y. Liu, W. C. H. Choy, L. Jin, Y. P. Leung, G. Zheng, J. Wang, A. K. Soh, *J. Phys. Chem. C* **2007**, *111*, 9055.

[8] J. Q. Hu, Y. Bando, J. H. Zhan, Z. W. Liu, D. Golberg, S. P. Ringer, *Adv. Mater.* **2005**, *17*, 975

[9] J. Q. Hu, Y. Bando, D. Golberg, *Small* **2005**, *1*, 95;

[10] a) Q. Peng, Y. J. Dong, Y. D. Li, *Angew. Chem.* **2003**, *115*, 3135; *Angew. Chem. Int. Ed.* **2003**, *42*, 3027; b) W. T. Yao, S. H. Yu, J. Jiang, L. Zhang, *Chem. Eur. J.* **2006**, *12*, 2066.

[11] a) X. G. Gou, F. Y. Cheng, Y. H. Shi, L. Zhang, S. J. Peng, J. Chen, P. W. Shen, *J. Am. Chem. Soc.* **2006**, *128*, 7222; b) S. L. Xiong, B. J. Xi, C. M. Wang, D. Xu, X. Feng, Z. Zhu, Y. Qian, *Adv. Funct. Mater.* **2007**, *17*, 2728; c) S. Xiong, B. Xi, C. Wang, G. Zou, L. Fei, W. Wang, Y. Qain, *Chem. Eur. J.* **2007**, *13*, 3076.

[12] a) J. Yang, C. Xue, S. Yu, J. H. Zeng, Y. Qian, *Angew. Chem.* **2002**, *114*, 4891; *Angew. Chem. Int. Ed.* **2002**, *41*, 4697; b) Z. X. Deng, C. H. Wang, X. M. Sun, Y. D. Li, *Inorg. Chem.* **2002**, *41*, 869; c) W. T. Yao, S. H. Yu, L. Pan, J, Li, Q. S. Wu, L. Zhang, J. Jiang, *Small* **2005**, *1*, 320; d) W. T. Yao, S. H. Yu, X. Y. Huang, J. Jiang, *Adv. Mater.* **2005**, *17*, 2799.

[13] a) X. Y. Huang, J. Li, Y. Zhang, A. Mascarenhas, *J. Am. Chem. Soc.* **2003**, *125*, 7049; b) Z. X. Deng, L. B. Li, Y. D. Li, *Inorg. Chem.* **2003**, *42*, 2331.

[14] a) X. G. Peng, L. Manna, W. D. Yang, J. Wickham, E. Scher, A. Kadavanich, A. P. Alivisatos, *Nature* **2000**, *404*, 59; b) N. Cordente, M. Respaud, F. Senocq, M. J. Casanove, C. Amiens, B. Chaudret, *Nano Lett.* **2001**, *1*, 565; c) Y. W. Jun, S. M. Lee, N. J. Kang, J. Cheon, *J. Am. Chem. Soc.* **2001**, *123*, 5150.

[15] S. Mann, H. Cölfen, *Angew. Chem.* **2003**, *115*, 2452; *Angew. Chem. Int. Ed.* **2003**, *42*, 2350.

[16] a) C. Z. Wu, Y. Xie, L .Y. Lei, S. Q. Hu, C. Z. OuYang, *Adv. Mater.* 2006, 18, 1727; b) C. L. Yan, D. F. Xue, *J. Alloys Compd.* **2007**, *431*, 241.

[17] M. V. Nazarov, *Mater. Sci. Eng. B* **2002**, *91*, 349.

[18] a) S. Fujita, H. Mimoto, T. Naguchi, *J. Appl. Phys.* **1979**, *50*, 107; b) N. Sankar, K. Ramachandran, *J. Cryst. Growth* **2003**, *247*, 157; c) A. Bukaluk, M. Trzcinski, F. Firszt, S. Legowski, H. Meczynska, *Surf. Sci.* **2002**, *507–510*, 175.

Received: May 29, 2008
Published online: September 12, 2008

 © 2008 Wiley-VCH Verlag GmbH & Co. KGaA, Weinheim